The RNA-binding protein HuR impairs adipose tissue anabolism in pancreatic cancer cachexia

Paige C. Arneson-Wissink[1,2], Katherine Pelz[1,3], Beth Worley[1], Heike Mendez [1,2], Peter Pham [1,2], Grace McCarthy [1,3], Alex Chitsazan[4], Jonathan R. Brody [1,3,5], Aaron J. Grossberg*[1,2,4,5]

[1]Brenden-Colson Center for Pancreatic Care, Oregon Health & Science University, Portland, OR

[2]Department of Radiation Medicine, Oregon Health & Science University, Portland, OR

[3]Department of Surgery, Oregon Health & Science University, Portland, OR

[4]Cancer Early Detection Advanced Research Center, Oregon Health & Science University, Portland, OR

[5]Department of Cell, Developmental, and Cancer Biology, Oregon Health & Science University, Portland, OR

***Corresponding Author**: Aaron J. Grossberg, 3181 SW Sam Jackson Park Rd Mail Code L481, Oregon Health and Science University, Portland, OR, 97239, 503-494-9945, grossber@ohsu.edu

ABSTRACT

Background: Cachexia is defined by chronic loss of fat and muscle, is a frequent complication of pancreatic ductal adenocarcinoma (PDAC), and negatively impacts patient outcomes. Nutritional supplementation cannot fully reverse tissue wasting, and the mechanisms underlying this phenotype are unclear. This work aims to define the relative contributions of catabolism and anabolism to adipose wasting in PDAC-bearing mice. Human antigen R (HuR) is an RNA-binding protein recently shown to suppress adipogenesis. We hypothesize that fat wasting results from a loss of adipose anabolism driven by increased HuR activity in adipocytes of PDAC-bearing mice.

Methods: Adult C57BL/6J mice received orthotopic PDAC cell (*Kras*^{G12D}*; p53*$^{R172H/+}$*; Pdx1-cre*) (OT-PDAC) or PBS (sham) injections. Mice exhibiting moderate cachexia (9 days after injection) were fasted for 24h, or fasted 24h and refed 24h before euthanasia. A separate cohort of PDAC mice were treated with an established HuR inhibitor (KH-3, 100 mg/kg) and subjected to the fast/refeed paradigm. We analyzed body mass, gross fat pad mass, and adipose tissue mRNA expression. We quantified lipolytic rate as the normalized quantity of glycerol released from 3T3-L1 adipocytes *in vitro*, and gonadal fat pads (gWAT) *ex vivo*.

Results: 3T3-L1 adipocytes treated with PDAC cell conditioned media (CM) liberated less triglyceride into the culture media than control-treated adipocytes (-28.1%) and had lower expression of lipolysis and lipogenesis genes than control cells. PDAC gWAT cultured *ex vivo* displayed decreased lipolysis compared to sham gWAT (-54.7%). PDAC and sham mice lost equivalent fat mass after a 24h fast, however, PDAC mice could not restore inguinal fat pads (iWAT) (-40.5%) or gWAT (-31.8%) mass after refeeding. RNAseq revealed 572 differentially expressed genes in gWAT from PDAC compared to sham mice. Downregulated genes

(n=126) were associated with adipogenesis (adj p=0.05), and expression of adipogenesis master regulators *Pparg* and *Cebpa* were reduced in gWAT from PDAC mice. Immunohistochemistry revealed increased HuR staining in gWAT (+74.9%) and iWAT (+41.2%) from PDAC mice. Inhibiting HuR binding restored lipogenesis in refed animals with a concomitant increase in iWAT mass (+131.7%) and genes regulating adipogenesis (*Pparγ*, *Cebpa*, *Retn*, *Adipoq*, *Fasn*).

Conclusions: Our work highlights deficient adipose anabolism as a driver of wasting in 3T3-L1 adipocytes treated with PDAC conditioned media and OT-PDAC mice. The small molecule KH3, which disrupts HuR binding, was sufficient to restore adipogenic and lipogenic gene expression and prevent adipose wasting. This highlights HuR as a potentially targetable regulatory node for adipose anabolism in cancer cachexia.

Key words: pancreatic ductal adenocarcinoma, cachexia, adipose, adipogenesis, HuR

INTRODUCTION

Cancer-associated cachexia is a wasting condition characterized by systemic inflammation, progressive weight loss, and atrophy of white adipose tissue (WAT) and skeletal muscle[1-3]. In addition to physical deterioration, individuals with cachexia also exhibit fatigue, anorexia, and cognitive decline[1-4], which contribute significantly to reductions in quality of life, ability to tolerate chemotherapy or surgery, and patient mortality[5-9]. Cachexia is estimated to be the direct cause of death in 20-30% of cancer patients[5, 6], and among all malignancies, pancreatic ductal adenocarcinoma (PDAC) is the most highly associated with cachexia, with an estimated 83% of patients suffering from this condition[10-12]. Despite much of cachexia research focusing on improving skeletal muscle mass, a retrospective study of patients with PDAC revealed that fat loss alone is associated with equally poor outcomes as combined muscle and fat mass loss [13]. Additionally, current cachexia clinical trials center around weight maintenance or gain as a primary endpoint. This highlights the importance of understanding the drivers of adipose tissue loss in cachexia.

Cachexia arises when energy catabolism exceeds anabolism, leading to unsustainable levels of fat mobilization and muscle depletion. Multiple factors are known to enhance catabolism, including decreased secretion of anabolic hormones, and altered metabolism of protein, carbohydrate, and lipid substrates[14]. Current work suggests that inflammation drives metabolic abnormalities in cachexia[10, 15]. Pro-inflammatory cytokine activity increases during cancer progression[16, 17] and systemic inflammation can contribute to wasting by inducing hypercatabolism in muscle and adipose tissue [14, 18-20]. Existing literature highlights elevated rates of lipolysis and adipose browning as the primary forces underlying adipose tissue wasting [21, 22]. Browning, in particular, appears to exert a double effect in

81 cachexia by both reducing lipid stores and increasing energy expenditure[22]. However,
82 impaired anabolic processes, like adipogenesis and lipogenesis, also contribute to adipose
83 tissue loss [23]. Targeting peroxisome proliferator-activated receptor gamma (PPARG), a
84 transcriptional control point of adipogenesis, with the agonist rosiglitazone was sufficient to
85 improve fat and muscle mass retention in mice with lung cancer [24]. Tumor-derived factors
86 are also capable of impairing adipogenesis in cultured 3T3L-1 adipocytes [25, 26].
87 RNA-binding proteins (RBPs) are essential in governing biogenesis, stabilization,
88 translation, and decay of mRNA transcripts[27, 28]. Several RBPs regulate alternative splicing
89 in adipocytes[29-31] and promote white adipose tissue browning [32] by inhibiting the
90 translation efficiency of mitochondrial mRNAs such as UCP1[33]. Until recently, the function of
91 most RBPs in adipocytes was largely unexplored. Recent work demonstrated that the RBP
92 human antigen R (HuR), encoded by the embryonic lethal abnormal vision-like 1 (*ELAVL1*)
93 gene, which regulates the expression of genes involved in inflammation, stress response, and
94 apoptosis, is also a repressor of adipogenesis in both white and brown adipose tissues[34, 35].
95 Our goal was to elucidate the relative contributions of enhanced catabolism and impaired
96 anabolism on fat wasting by investigating adipose tissue response to different nutritional
97 contexts and HuR inhibition in cachectic mice.

98 **METHODS**

99 *Cell culture*

100 *KPC PDAC cells*

101 KPC cells expressing pancreas-specific conditional alleles (*Kras*^{G12D}*; p53*$^{R172H/+}$*; Pdx1-*
102 *cre*)[36] were stored in liquid nitrogen until use and then maintained in RMPI 1640
103 supplemented with 10% FBS, 1mM sodium pyruvate, and 50 U/mL penicillin/streptomycin

104 (Gibco, Gaithersburg, MD) at 37C and 5% CO_2. Conditioned media (CM) was collected from
105 confluent KPC cells grown in DMEM, 1% pen/strep (to accommodate later culturing of 3T3-L1
106 cells) after 24 hours incubation, centrifuged at 1,200 g for 10 min, filtered with a 0.2-μm syringe
107 filter, and used immediately or stored at −80°C.

108 *3T3-L1 adipocytes*

109 3T3-L1 adipocytes (ATCC CL-173) were purchased from ATCC and stored in liquid
110 nitrogen until use. Cells were first treated with preadipocyte expansion media (DMEM, 10%
111 bovine calf serum, 1% pen/strep) for 3-4 days. Then, cells were plated at a density of $2x10^5$
112 cells/6-well dish, or 6.7 $x10^3$ cells/96well dish and maintained in preadipocyte expansion media
113 for 2 days after reaching 100% confluency. Media was changed to adipocyte differentiation
114 media (DMEM, 10% FBS, 1% pen/strep, 1 uM dexamethasone, 0.5 mM IBMX, 1 ug/mL bovine
115 insulin) for 2 days before switching to adipocyte maintenance media (DMEM, 10% FBS, 1%
116 pen/strep, 1 ug/mL bovine insulin) for the duration of the experiment. Cells were cultured for up
117 to 6 days after start of maintenance media. CM was added in place of adipocyte maintenance
118 media and was supplemented with FBS and insulin.

119 *Oil red O staining*

120 Diluted Oil Red O stock solution was prepared by mixing concentrated Oil Red O (0.5%
121 Oil Red O in 100% isopropyl alcohol) 6:4 with deionized water. This solution was allowed to
122 stand for 10 minutes at 4C and then filtered immediately before use through a 0.22 um filter.
123 3T3-L1 cells were washed with PBS, then incubated in 4% paraformaldehyde for 30 minutes at
124 room temperature, then washed with deionized water twice. Cells were incubated in 60%
125 isopropyl alcohol for 5 minutes, then treated with diluted Oil Red O solution for 15 minutes.

126 Cells were washed 5 times with deionized water, then red signal was quantified at 490 nm in a
127 plate reader (BioTek).

128 *Triglyceride quantification*

129 3T3-L1 mature adipocytes were treated with KPC CM or control media for 24 hours,
130 then media was collected off of 3T3-L1 cells for triglyceride quantification according to
131 manufacturer instructions (Stanbio Liquicolor Triglycerides Assay #2100, Fisher Scientific).
132 Absorbance was read at 500 nm on a plate reader (BioTek).

133 *Mouse studies*

134 Wildtype C57BL/6J mice (JAX catalog number 000664) were purchased from The
135 Jackson Laboratory (Bar Harbor, ME) and maintained in standard rodent housing at 26°C with
136 12h light/12h dark cycles. Animals used for experimentation were 12-15 weeks of age. Mice
137 were individually housed for acclimation for 7 days prior to tumor implantation and provided *ad*
138 *libitum* access to water and food (Rodent diet 5001; Purina Mills, St. Louis, MO, USA). Food
139 intake was measured daily. Tumor-bearing animals were euthanized by cardiac puncture
140 under deep isoflurane anesthesia. Studies were conducted in accordance with the U.S.
141 National Institutes of Health Guide for the Care and Use of Laboratory Animals and approved
142 by the Institutional Animal Care and Use Committee of Oregon Health & Science University.

143 *Study-specific manipulations*

144 For fasting studies, mice were transferred to clean cages without food for 24 hours prior
145 to euthanasia or refeeding. Pair-feeding was used on the study days indicated in the figure
146 legends by feeding sham mice the average of the food consumed by PDAC mice the day prior.
147 PDAC mice treated with the HuR inhibitor KH3, were injected intraperitoneally (100 mg/kg) at
148 6-, 8-, and 10-days post-implantation.

149 *Orthotopic PDAC implantation*

150 Wildtype C57BL/6J mice aged 12-15 weeks received orthotopic PDAC tumor injections
151 (*Kras*^{G12D}*; p53*$^{R172H/+}$*; Pdx1-cre*) or sham injections. PDAC mice were injected with 1x10^{6} KPC
152 cells into the tail of the pancreas parenchyma in a volume of 23ul while sham animals were
153 treated with an equal volume of PBS. Animals were euthanized 10-11 days after tumor
154 implantation. N and sex are defined on a per-study basis in the figure legends.

155 *Echo magnetic resonance imaging body composition*

156 Lean mass, fat mass, total body water, and free water were measured using whole-
157 body magnetic resonance imaging (MRI) (EchoMRI, Houston, TX). Measurements were taken
158 pre-implantation, pre-fasting and at euthanasia in tumor and sham groups to assess body
159 composition.

160 *Tissue collection and histology*

161 Tissues collected at necropsy were weighed and flash frozen in liquid nitrogen prior to
162 storage at -80C. Tissues for HuR histology were fixed with 4% paraformaldehyde overnight
163 and then transferred to 70% ethanol. Tissues were paraffin-embedded, sectioned, incubated
164 with anti-HuR (1:300 #sc-5261, Santa Cruz Biotechnology Inc, Dallas, TX) and stained using
165 horseradish peroxidase-conjugated secondary antibody and incubation in 3,3'-
166 diaminobenzidine by the Histopathology Shared Resource Core at OHSU. Whole tissue
167 sections were scanned by the Advanced Light Microscopy Core at OHSU. ZEN Digital Imaging
168 for Light Microscopy (RRID:SCR_013672) was then used to obtain at least five 10x images per
169 tissue. ImageJ software was used to quantify the percent staining for each section (56). All
170 staining was quantified by running color deconvolution on 10x images, applying a standard

171 intensity threshold on the corresponding images, and measuring the percent area covered by
172 the staining.

173 *Ex vivo lipolysis*

174 *Ex vivo* lipolysis assays of adipose explants were performed as previously
175 described[37]. Briefly, gonadal white adipose tissue (gWAT) tissue was collected and cut into
176 approximately 100 mg samples, minced, then incubated in phenol red-free DMEM containing
177 2% fatty acid free bovine serum albumin at 37°C for 1 hour. Media was collected and snap-
178 frozen. The tissue was transferred to a new dish containing media only or media with 10 uM
179 isoproterenol and incubated for 2 hours at 37C. Media was collected and snap-frozen. Media
180 aliquots were thawed and analyzed for glycerol using Sigma Glycerol Assay Kit (MAK117)
181 according to manufacturer's directions.

182 *Quantitative qRT-PCR*

183 Total RNA was extracted from cell pellets or tissues with the E.Z.N.A. Total RNA Kit II
184 (Omega Bio-Tek Inc., Norcross, GA). cDNA was transcribed with the High-Capacity cDNA
185 Reverse Transcription Kit (Applied Biosystems, Waltham, MA). Quantitative real-time
186 polymerase chain reaction (qPCR) was run on the ABI 7300 (Applied Biosystems) using
187 TaqMan Fast Advanced PCR Master Mix (Applied Biosystems) or SYBR Green Master Mix
188 (Applied Biosystems). The relative expression was calculated using the $\Delta\Delta C_t$ method with
189 gene expression relative to beta actin or 18S.

190 *RNA sequencing*

191 RNA sequencing was performed on total RNA isolated as described above. RNA
192 libraries were prepared and sequenced using the Illumina Nova Seq and HiSeq platform
193 according to the Illumina Tru-Seq protocol (Novogene, Sacramento, CA). Reference genome

194 and gene model annotation files were downloaded from genome website browser
195 (NCBI/UCSC/Ensembl) directly. FASTQ files obtained from sequencing were put through fastp
196 to trim adapters and then fastqc for quality analysis. STAR 2.7.1a was then used to align to
197 reference genome (mm10) to trimmed reads after which htseq was used to obtain gene
198 counts. Raw reads were normalized using DESeq2 (1.38.3). Genes with an adjusted *P*-value
199 <0.05 found by DESeq2 were assigned as differentially expressed. Gene set enrichment
200 analysis (GSEA) was performed through the Broad Institute GUI. Normalized counts from
201 DESeq2 from gWAT were input and analyzed with relationship to the Molecular Signature
202 Database (msigdb). Significant Hallmark genes (p <0.05) were graph from both positive and
203 negative normalized enrichment scores (NES). Log2 fold change, p-values and p-adj from
204 differential expression data obtained through deseq2 were loaded into Qiagen's Ingenuity
205 Pathway Analysis (IPA) to look at upstream and downstream regulators. Volcano plots created
206 from differential expression data of pairwise comparison with sham groups being baseline
207 using ggplot2 (3.5). Significant genes from adipogenesis pathway are labeled. Heatmaps were
208 created of genes in the adipogenesis pathway regardless of significance using
209 pheatmap(1.0.12).

210 ***Statistical Analysis***

211 Specific statistical tests and sample size for each study is indicated in the figure
212 legends. Error bars in figures show SEM. Statistical analyses were performed using GraphPad
213 Prism (version 9; GraphPad Software Inc), and graphs were built using GraphPad Prism
214 (GraphPad Software Inc) statistical analysis software or R studio (4.2.3) using ggplot (3.5.1). P
215 values are 2 sided with values less than 0.05 regarded as statistically significant.

216 ***Data Availability***

217 Further information and resources, including KPC cells and raw data will be shared
218 upon reasonable request to Aaron J. Grossberg (grossber@ohsu.edu).
219
220 **RESULTS**
221 **Adipocytes suppress lipogenesis in response to PDAC-derived factors**
222 Given a large body of literature suggesting that PDAC cachexia is partly driven by
223 increased lipolysis in the adipose tissue, we tested the effect of PDAC cell conditioned media
224 (KPC CM) on lipolysis *in vitro* [21, 22, 38]. We treated differentiated 3T3-L1 cells with control
225 maintenance media, or with KPC CM for 6 days. At this time, we observed decreased lipid
226 droplet accumulation by brightfield microscopy, which was confirmed with Oil Red O (**Figure**
227 **1A-B**). Liberated triglyceride (TG) levels, a measure of lipolysis, were significantly lower in the
228 media of KPC CM-treated cells (**Figure 1C**). Correspondingly, mRNA levels of lipolysis
229 enzymes adipose triglyceride lipase (*Atgl*) and lipase E (*Lipe*) were significantly decreased in
230 KPC CM-treated 3T3-L1 cells (**Figure 1D**). To explain the apparent decrease in lipid
231 accumulation without increased lipolysis, we measured the expression of genes associated
232 with lipogenesis: fatty acid synthase (*Fasn*), nuclear receptor subfamily 1 group H member 3
233 (*Nr1h3*), solute carrier family 2 member 4 (*Slc2a4*), and lipoprotein lipase (*Lpl*). All of these
234 genes were suppressed after KPC CM treatment, indicating that the decreased lipid content in
235 3T3-L1 cells was due to impaired anabolic activity rather than increased catabolic activity
236 (**Figure 1E**).
237 **PDAC is associated with decreased fat pad mass *in vivo***
238 We first sought to assess the effects of pancreatic cancer on metabolism by
239 characterizing tissue physiology in a murine orthotopic PDAC model. 12-week-old C57BL/6J

240 mice with PDAC or sham implantations were fed *ad libitum* with or without a 24h fast once
241 mice reached a moderate cachexia burden (9 days after tumor implantation). Body mass
242 maintained stable among all groups prior to fasting (**Figure 2A**), whereas PDAC mice
243 exhibited a small reduction in food intake (**Figure 2B**) compared to sham controls. EchoMRI
244 body composition analysis of fat mass demonstrated significant decreases in overall adiposity
245 in PDAC animals from baseline to pre-fast due to cachexia progression and reduction in food
246 intake (**Figure 2C**). As expected, between pre- and post-fast, both PDAC and sham animals
247 lost significant overall adiposity (**Figure 2D**). Terminal fat pad mass in fasted PDAC animals
248 was not significantly altered compared to fasted sham mice (**Figure 2E**), indicating that both
249 groups exhibit similar rates of fasting-induced lipolysis. Fasting caused a significant reduction
250 in tumor mass compared to *ad libitum*-fed mice (**Figure 2F**).

251 **PDAC impairs lipolysis and adipogenesis**

252 Based on our findings *in vitro*, we hypothesized that PDAC mice would not exhibit
253 increased lipolysis, which is characteristic of other cachexia models [21, 38]. To measure the
254 rate of adipose tissue catabolism, we performed an *ex vivo* lipolysis study, using gonadal white
255 adipose tissue (gWAT) collected from sham and PDAC mice. We assessed fat pads both in
256 the presence and absence of the beta-adrenergic agonist isoproterenol (10 uM) to determine
257 baseline and stimulated lipolysis[39]. Baseline and isoproterenol-stimulated glycerol release
258 were significantly decreased in PDAC gWAT (**Figure 3A**), demonstrating that PDAC
259 suppresses, rather than enhances, lipolytic rate and capacity. To further characterize the
260 molecular biology of adipocytes during PDAC, we assessed mRNA expression of genes
261 regulating lipolysis and browning in adipose tissue. PDAC mice failed to increase gWAT and
262 inguinal white adipose tissue (iWAT) *Atgl* and *Lipe* expression in response to fasting (**Figure**

263 **3B**). We observed similar decreases in browning-associated gene expression, including
264 peroxisome proliferator-activated receptor gamma coactivator 1 alpha (*Pgc1a),* protein domain
265 containing 16 (*Prdm16*), and cell death inducing DFFA like effector a (*Cidea*) in PDAC mice in
266 both *ad libitum* fed and fasted conditions. Uncoupling protein 1 (*Ucp1*), which is also
267 associated with browning, was not significantly increased in gWAT from PDAC mice (**Figure**
268 **3B-C**). Therefore, neither enhanced lipolysis nor browning are significant contributors to
269 adipose loss in this model.

270 **PDAC downregulates pathways associated with adipogenesis**

271 To gain further insights into PDAC metabolism from global gene expression analysis,
272 we performed bulk RNA sequencing (RNAseq) on gWAT from sham and PDAC animals. . In
273 gWAT, we identified a total of 572 differentially expressed genes (DEGs) in PDAC versus
274 sham mice, of which 446 were enriched, and 126 were depleted (**Figure 4A, S1**). Pathway
275 analysis referencing the molecular signatures database (MSigDB) hallmark gene set collection
276 revealed increased expression of gene sets associated with cell cycle control (e.g., E2F
277 targets and G2M checkpoints) and inflammation (e.g. TNFa and JAK/STAT3 signaling) and
278 decreased expression of genes linked to adipogenesis, oxidative phosphorylation, and fatty
279 acid metabolism (**Figure 4B**)[40]. Because inhibition of adipogenesis could provide an
280 alternative mechanism for adipose wasting, we plotted all significant DEGs in the adipogenesis
281 gene set and observed nearly universal depletion of these transcripts in PDAC mice (**Figure**
282 **4C**). We then validated our RNAseq data by performing qPCR on selected adipogenesis-
283 associated DEGs, revealing consistent downregulation of both adipogenesis and lipogenesis
284 genes (**Figure 4D**). We then repeated qPCR in iWAT to determine whether subcutaneous
285 adipose exhibited the same transcriptomic changes. Transcriptional changes in iWAT were

286 less dramatic than in gWAT and did not reach significance, with the exception of *Lpl*, which
287 was significantly decreased in PDAC tissue (**Figure 4E**). Together, these results indicate that
288 suppressed transcriptomic programs associated with adipogenesis could account for
289 decreased adipose tissue during cachexia, in the absence of elevated lipolysis.

290 **Adipose tissue anabolism is impaired in orthotopic PDAC mice after refeeding**

291 Based on our results demonstrating downregulation of adipogenic and lipogenic genes
292 in PDAC mice, we next wanted to confirm whether adipose tissue anabolism is functionally
293 impaired in mice implanted with orthotopic PDAC. To do this, wildtype C57BL/6J mice with
294 PDAC or sham implantations were fed *ad libitum* for 9 days, an established timepoint of active
295 cachexia[41], fasted 24h, and then terminated or allowed to re-feed for 24 h. To control for
296 differences in caloric intake, we used a pair-fed refeeding scheme in which sham mice were
297 refed with the average food consumption of the refed PDAC group. Challenging mice with a
298 24h fast depletes adipose mass equally in PDAC and sham mice (**Figure 2D**), enabling us to
299 assess anabolic restoration of fat mass during a 24 h refeeding period. We observed
300 measured cumulative food intake and daily body mass for the duration of the study (**Figure**
301 **5A-B**). Fasting and refeeding did not impact pancreas tumor mass (**Figure S2**). There were no
302 differences in iWAT or gWAT mass in fasted PDAC versus sham mice (**Figure 5C-D**).
303 However, while sham mice regain significant amounts of gWAT and iWAT mass after
304 refeeding, gWAT and iWAT masses in PDAC mice remain equivalent before and after
305 refeeding (**Figure 5C-D**). Refeeding sham mice caused increased gWAT expression of
306 lipogenic *Fasn* and adipogenic genes *Lep* and *Retn*, while these genes remained suppressed
307 in PDAC gWAT (**Figure 5E**). Refed sham iWAT showed increased *Fasn,* but not adipogenic
308 genes, while PDAC iWAT had suppressed expression of both adipogenic and lipogenic genes

309 (**Figure 5F**). These results confirm that downregulation in pathways mediating adipogenesis
310 are indeed accompanied by impaired adipose tissue anabolism in orthotopic PDAC mice after
311 refeeding.

312 **HuR is overexpressed in orthotopic PDAC fat tissue**

313 Following our observation that adipose tissue anabolism is impaired in PDAC animals,
314 we next sought to understand the mechanism of this phenomenon. We used Ingenuity
315 Pathway Analysis upstream regulator analysis to identify potential candidates that could drive
316 impaired anabolism in PDAC adipose tissue. From the DEGs identified in gWAT of PDAC
317 mice, we found that canonical regulators of adipogenesis, such as troglitazone, fenofibrate,
318 PPARA, and PGC1A, were predicted to be inhibited. Inflammatory cytokines associated with
319 PDAC and cachexia, such as MYD88, IL-6, TNFA, IFNG, and IL-1B, were predicted to be
320 activated. Among other targets that were predicted to be activated but were not typically
321 associated with cachexia was human antigen R (HuR, *ELAVL1*), an RNA-binding protein
322 recently established as a suppressor of adipogenesis[34] (**Figure 6A**). Given the predicted
323 activation of HuR in gWAT and existing literature, we next asked if HuR was more abundant in
324 adipose tissue from PDAC mice. We performed immunohistochemical staining of HuR in
325 formalin-fixed, paraffin-embedded sham and PDAC gWAT, iWAT, pancreas, and muscle
326 tissue. HuR staining was significantly increased in both the gWAT and iWAT of PDAC mice
327 versus sham controls (**Figure 6C-D, S4).** We also observed increased HuR staining in the
328 pancreas, but not skeletal muscle from PDAC mice, as compared to sham controls (**Figure**
329 **6B, S3**).

330 **HuR inhibition improves metabolic deficits and restores adipogenesis *in vivo***

331 Since HuR has been established as driving pro-survival pathways in PDAC, we next
332 wanted to determine if preventing HuR binding to target mRNAs could reverse adipose wasting
333 in PDAC cachexia[35]. To do this, we treated PDAC mice with a selective HuR inhibitor, KH-3,
334 which prevents binding of HuR to its target mRNA sequence[42]. All mice received orthotopic
335 PDAC tumor injections and were fed *ad libitum* then fasted 24h with or without a 24h refeed at
336 mid-cachexia (9 days after injection). In each feeding group, mice were treated with the HuR
337 inhibitor KH-3 (100 mg/kg) or vehicle at 6-, 8-, and 10-days post-injection. Cummulative food
338 intake between vehicle and KH3 groups was not statistically significant prior to fast. KH3
339 treated PDAC mice gained significantly more weight during refeeding compared to vehicle-
340 treated mice (**Figure 7A-B**). Refeeding was associated with larger tumors in both vehicle and
341 KH-3 groups, likely due to both log growth and the propensity for mice to become dehydrated
342 during fasting (**Figure 7C**). KH-3 treatment itself had no effect on tumor growth over this time
343 interval. KH-3 treatment caused a nonsignificant increase in gWAT mass and significantly
344 increased iWAT mass in refed animals (**Figure 7D-F**). In contrast, vehicle-treated mice did not
345 significantly increase fat pad mass during refeeding. This effect is specific to adipose tissue, as
346 gastrocnemius muscle mass was not changed between fast/refeed, or vehicle/KH-3 treatment
347 (**Figure 7F**). To molecularly test the impact of HuR inhibition on adipogenesis and lipogenesis
348 gene expression, we analyzed gWAT and iWAT tissues by qPCR. KH-3 treatment successfully
349 restored expression of adipogenic (*Cebpa, Adipoq, Lep*, *Retn*) and lipogenic (*Fasn*) genes
350 (**Figure 8A-B, D-E**). HuR inhibition did not impact lipolysis gene expression (*Atgl* and *Lipe*)
351 (**Figure 8C, F**). Thus, we show a role for HuR in adipose tissue metabolism during PDAC-
352 associated cachexia, whereby inhibiting HuR successfully ameliorates adipose tissue wasting
353 *in vivo* by restoring the expression of genes associated with adipogenesis and lipogenesis.

354 **DISCUSSION**

355 This work evaluates the relative contributions of enhanced catabolism and impaired
356 anabolism on fat wasting by investigating adipose tissue response to different nutritional
357 contexts and HuR inhibition in cachectic mice. We demonstrate that our murine model of
358 PDAC cachexia exhibits a near-complete deficit in adipose tissue anabolism in the context of
359 reduced lipolysis, which corroborates a growing set of literature that challenges the dogma that
360 fat wasting occurs as a result of only enhanced catabolism[24-26]. We further identify HuR as
361 a potential molecular mediator of adipogenesis during pancreatic cancer progression.
362 Collectively, these studies support other work describing heterogeneity within cancer-
363 associated cachexia that could have major implications on therapeutic strategies moving
364 forward [13, 43]. In the future, clinical trials may see more therapeutic success if they employ
365 patient selection based on patients' underlying mechanisms of wasting.

366 Our study implicates the RNA-binding protein HuR in the inhibition of adipogenesis and
367 lipogenesis in adipose tissue. HuR can impact the transcriptome through both RNA binding
368 and HuR-dependent splicing [35]. One documented mechanism of HuR-mediated
369 adipogenesis regulation is via HuR binding to adipogenesis upstream regulator *Pparg*, which
370 suppresses *Adipoq* protein expression in a non-transcriptionally dependent manner [44]. In our
371 RNA sequencing, we did not observe increased HuR expression, although others have
372 documented increased HuR expression in response to nuclear factor-kappa B (NF-κB)
373 signaling[45]. Alternatively, we identified HuR as an upstream regulator based on adipose
374 transcriptomic changes associated with PDAC. In this context, HuR is more likely controlled
375 post-translationally, although further investigation is needed to identify the specific PDAC-
376 associated factors that may activate HuR stability and nuclear translocation [46].

377 Small molecule antagonists of HuR, such as KH-3, are currently in development and
378 have been found to have anti-tumor effects[35, 47]. In our studies, KH-3 ameliorated anti-fat
379 wasting but also induced severe hemolytic anemia in all treated mice. Tumor size was not
380 impacted by KH3 treatment, likely because of the short period of dosing. However, studies
381 aimed to evaluate tumor growth over 5 weeks documented slower tumor growth and fewer
382 metastases in KH-3-treated mice [48]. In our studies, the anti-cachectic effects of KH-3 were
383 specific to adipose tissue and did not preserve skeletal muscle mass. Although prior studies
384 link muscle and adipose wasting, these models are all characterized by enhanced lipolysis and
385 browning [38]. In our model, adipose and muscle wasting appear to be driven by independent
386 mechanisms. Continued improvement of HuR antagonists could lead to therapeutics that
387 restore anabolic potential in adipose tissue, providing a novel approach to alleviating one
388 symptom of cachexia, while also providing anti-tumor benefits.
389 In addition to impaired anabolic potential in adipose tissue, our PDAC model also
390 presents suppressed lipolysis. Suppressed lipolysis could contribute to systemic defects in
391 energy utilization in cancer cachexia. Prior work from our group shows that PDAC impairs
392 hepatic lipid oxidation but that this does not result in lipid accumulation or fatty liver [41]. While
393 hepatic metabolic deficits were not HuR dependent, it is possible that impaired lipid
394 mobilization contributes to global metabolic disruption. Further interrogation is needed to
395 understand how improved fat retention through HuR inhibition might impact lipid mobilization
396 and systemic metabolism.

397 **ACKNOWLEDGEMENTS**

398 We thank all members of the Aaron Grossberg and Jonathan Brody labs for their helpful
399 discussion and suggestions. We also would like to thank Dr. Laing Xu (Department of

Molecular Biosciences, University of Kansas, Lawrence, Kansas) for generously providing us with the KH3 compound. Author contributions are: Conceptualization, KP, AJG. Methodology, KP, HM, PP, GM, AC, AJG. Validation, PCAW, KP, HM, BW, PP. Formal Analysis, PCAW, KP, HM, BW, PP, GM, AC, AJG. Investigation, PCAW, KP, HM, BW, PP, GM, AC. Writing—Original Draft, PCAW, BLW. Writing – Review and Editing, PCAW, PP, JB, AJG. Visualization, PCAW, KP, HM, BW, PP, GM, AC. Supervision, JB, AJG. Project Administration, JB, AJG. Funding Acquisition, JB, AJG. All authors approved this manuscript.

Funding: This work was supported by National Cancer Institute grants K99CA286709 (PCAW), R37CA280692 (AJG), R01264133 (AJG), and K08245188 AJG), R01 CA212600 (JRB), U01CA224012-03 (JRB), R21 CA263996 (JRB), AACR Grant-15-90-25-BROD (JRB), the Hirshberg Foundation (JRB), and support from the Brenden Colson Center for Pancreatic Care (AJG, JRB, and PCAW). This work is also supported by the Histopathology Shared Resource for pathology studies (University Shared Resource Program at Oregon Health and Sciences University and the Knight Cancer Institute (P30 CA069533 and P30 CA069533 13S5)).

Conflict of interest: The authors do not declare any conflicts of interest.

Ethical standards: The authors of this manuscript certify that they comply with the ethical guidelines for authorship and publishing in the Journal of Cachexia, Sarcopenia and Muscle.[49] All human and animal studies were approved by the appropriate ethics committees and were therefore performed in accordance with the ethical standards laid down in the 1964 Declaration of Helsinki and its later amendments. All human subjects provided informed consent and any identifying information of individual patients has been omitted.

FIGURE LEGENDS

Figure 1: Adipocytes suppress lipogenesis in response to pancreatic ductal adenocarcinoma-conditioned media. Differentiated 3T3-L1 adipocytes were cultured for 6 days in control or KPC CM, with the exception of the TG assay. **(A)** Brightfield images of differentiated 3T3-L1 cells treated with control media (right) or KPC CM (left). Scale bars represent 200 um. Representative of 3 wells per condition. **(B)** Quantification of Oil Red O staining. N = 4 wells per condition. **(C)** Media triglyceride levels after 24 hours of exposure to control or KPC CM. N=3 wells per condition. **(D)** mRNA expression lipolysis genes N= 3 wells per condition, normalized to 18S expression. **(E)** mRNA expression of lipogenesis genes. N= 3 wells per condition, normalized to 18S expression. Pairwise analyses tested with t-test. $p<0.05$, $^{**}p<0.01$, $^{***}p<0.001$, and $^{****}p<0.0001$.

Figure 2: Pancreatic ductal adenocarcinoma is associated with decreased fat pad mass *in vivo*. Wildtype C57BL/6J mice with PDAC or sham implantations were fed *ad libitum* or fasted 24h at mid-cachexia (9 days after injection). Animals were euthanized 10 or 11 days after tumor implantation following the 24h fast. N= 5 sham, 6 PDAC male mice per feeding condition. **(A)** Daily body mass. Statistically tested with 3-way ANOVA $p<0.0001$ for time, time x fast; $p=0.0073$ for fast; $p=0.0097$ for time x tumor status; $p=0.0167$ for tumor status. **(B)** Cumulative food intake. Statistically tested with 3-way ANOVA $p<0.0001$ for time, time x fast; $p=0.0035$ for time x tumor status. **(C-D)** Body composition changes in total adiposity were characterized at baseline to pre-fast between sham and PDAC mice **(C)**, and at pre- to post-fast **(D)**. MRI analyses were statistically tested with mixed effects model with Fisher's LSD test. **(E)** Terminal gWAT mass. **(F)** Terminal pancreas/tumor mass. 2x2 analyses were statistically tested with two-way ANOVA with Tukey multiple comparisons. $^{*}p<0.05$, $^{**}p<0.01$, and $^{****}p<0.0001$.

Figure 3: Pancreatic ductal adenocarcinoma impairs lipolysis and adipogenesis *in vivo*. **(A)** Measurement of lipolysis (glycerol release) in explants derived from gWAT collected 10 days post tumor implantation. Lipolysis was induced by the agonist isoproterenol (10 μM). N= 6 male mice per group. Statistically tested with two-way ANOVA with uncorrected Fisher's LSD test to compare groups. **(B)** mRNA expression lipolysis genes in gWAT collected 10 days post-implantation from 24h fasted and ad lib mice, normalized to 18S expression. N=5 male mice sham fasted; 3 male, 3 female mice sham ad lib; 6 male mice PDAC fasted; 3 male, 2 female mice PDAC ad lib. **(C)** mRNA expression of lipolysis genes in iWAT collected 11 days post-implantation from ad lib mice, normalized to beta actin expression. N= 4 male mice per group. 2x2 data were statistically tested with two-way ANOVA with Tukey multiple comparisons comparing tumor experimental groups to sham controls. Pairwise comparisons were made with unpaired t test. $^{*}p<0.05$, $^{**}p<0.01$, $^{***}p<0.001$, and $^{****}p<0.0001$.

Figure 4: PDAC downregulates pathways associated with adipogenesis. RNAseq on gWAT from ad lib fed PDAC and sham mice collected 14 days post tumor implantation. N = 2 female, 3 male PDAC; 3 female, 2 male sham. **(A)** Volcano plot of differentially expressed genes in gWAT. Blue dots represent significantly downregulated genes (log2FC < -1 and adj $p<0.05$). while red dots represent significantly upregulated genes (log2FC >1 and adj $p<0.05$). Grey dots are insignificant. Labels denote significant differentially expressed genes from the

Hallmark Adipogenesis pathway. **(B)** Broad Institute GSEA significantly enriched pathways in PDAC gWAT relative to sham gWAT (pathway pval <0.05). Blue is downregulated, red is upregulated. **(C)** Heat map of Hallmark Adipogenesis pathways constituents in PDAC and Sham gWAT. Scale represents row normalized raw counts. **(D)** qPCR validation of adipogenesis and lipolysis genes in in gWAT collected 10 days post-implantation from 24h fasted and ad lib mice. N=5 male mice sham fasted; 3 male, 3 female mice sham ad lib; 6 male mice PDAC fasted; 3 male, 2 female mice PDAC ad lib. Statistically tested with two-way ANOVA with Tukey multiple comparisons comparing tumor experimental groups to sham controls. **(E)** qPCR validation of adipogenesis and lipolysis genes in iWAT from ad lib fed mice collected 11 days post implantation. N = 4 male mice per group. Statistically tested with unpaired t test. *p<0.05, **p<0.01, ***p<0.001, and ****p<0.0001.

Figure 5: Adipose tissue anabolism is impaired in orthotopic PDAC mice after refeeding. Wildtype C57BL/6J mice with PDAC were fed *ad libitum* then fasted 24h or fasted 24h followed by a refeed at mid-cachexia (9 days after injection). Sham mice were pair-fed to PDAC average food intake from 2 days post-implantation until study end. Animals were euthanized 9 or 10 days after tumor implantation following the 24h fast or *ad libitum* refeed. N= 3 male and 3 female mice per group. **(A)** Cumulative food intake. Statistically tested with 3 way ANOVA. P<0.0001 for time, p=0.0344 for time x tumor status. **(B)** Daily body mass. Statistically tested with 3 way ANOVA. P<0.0001 for time, p=0.002 for time x tumor status. **(C)** iWAT mass normalized to initial body mass, normalized to beta actin expression. **(D)** gWAT mass normalized to initial body mass, normalized to beta actin expression. **(E)** mRNA expression of anabolic genes in gWAT. **(F)** mRNA expression of anabolic genes in iWAT. Data represented in C-F were statistically tested with two-way ANOVA with Tukey multiple comparisons comparing tumor experimental groups to sham controls. *p<0.05, and ****p<0.0001.

Figure 6: HuR is overexpressed in PDAC orthotopic pancreas and fat tissue. (A) Selected upstream regulator predictions from Ingenuity Pathway Analysis of differentially expressed genes in gWAT. **(B-D)** Representative images and quantification of immunohistochemical detection of HuR in tissue from PDAC and sham mice. **(B)** Pancreas N=4 male and 4 female mice per group. **(C)** gWAT N=4 male and 4 female mice per group. **(D)** iWAT N= 3 female, 2 male sham and 2 female, 3 male PDAC. Scale bars represent 100 um. Statistically tested with t test. *p<0.05, **p<0.01, ***p<0.001, and ****p<0.0001.

Figure 7: HuR inhibition prevents adipose tissue loss *in vivo*. Wildtype C57BL/6J mice with PDAC were fed *ad libitum* then fasted 24h or fasted 24h followed by a refeed at mid-cachexia (9 days after injection). In each feeding paradigm, groups were treated with either vehicle or the HuR antagonist, KH-3, then euthanized 10 or 11 days after tumor implantation following the 24h fast or *ad libitum* refeed. Vehicle-treated mice were pair-fed to the KH-3 treated group's average food intake from 8 days post-implantation until study end. N = 7 male mice per group. **(A)** Cumulative food intake, statistically tested as an unpaired t test of vehicle vs KH3 treatment at day 9 (prior to fast) p =0.1121. **(B)** Change in body weight after refeeding, statistically tested with unpaired *t* test. **(C)** Terminal pancreas mass. **(D)** Terminal gWAT mass. **(E)** Terminal iWAT mass. **(F)** Terminal gastrocnemius mass. 2x2 analyses were statistically tested with two-way ANOVA with Tukey multiple comparisons*p<0.05, and **p<0.01.

514 **Figure 8: HuR inhibition partially restores adipogenesis and lipogenesis *in vivo*. (A)**
515 mRNA expression of Adipogenesis genes in gWAT, normalized to beta actin expression. **(B)**
516 mRNA expression of lipogenesis genes in gWAT. **(C)** mRNA expression of lipolysis genes in
517 gWAT. **(D)** mRNA expression of Adipogenesis genes in iWAT, normalized to beta actin
518 expression. **(E)** mRNA expression of lipogenesis genes in iWAT. **(F)** mRNA expression of
519 lipolysis genes in iWAT. Data were statistically tested with two-way ANOVA with Tukey
520 multiple comparisons correction. N = 7 male mice per group. *$p<0.05$, **$p<0.01$, ***$p<0.001$,
521 and ****$p<0.0001$.
522

523

524 **REFERENCES**

525 1. Tisdale MJ. Biology of cachexia. J Natl Cancer Inst. 1997;89:1763-73.
526 doi:10.1093/jnci/89.23.1763
527 2. Grossberg AJ, Scarlett JM, Marks DL. Hypothalamic mechanisms in cachexia. Physiol
528 Behav. 2010;100:478-89. doi:10.1016/j.physbeh.2010.03.011
529 3. Baracos VE, Martin L, Korc M, Guttridge DC, Fearon KCH. Cancer-associated
530 cachexia. Nat Rev Dis Primers. 2018;4:17105. doi:10.1038/nrdp.2017.105
531 4. Olson B, Marks DL. Pretreatment Cancer-Related Cognitive Impairment-Mechanisms
532 and Outlook. Cancers (Basel). 2019;11:doi:10.3390/cancers11050687
533 5. von Haehling S, Anker MS, Anker SD. Prevalence and clinical impact of cachexia in
534 chronic illness in Europe, USA, and Japan: facts and numbers update 2016. J Cachexia
535 Sarcopenia Muscle. 2016;7:507-9. doi:10.1002/jcsm.12167
536 6. von Haehling S, Anker SD. Cachexia as a major underestimated and unmet medical
537 need: facts and numbers. J Cachexia Sarcopenia Muscle. 2010;1:1-5. doi:10.1007/s13539-
538 010-0002-6
539 7. Fearon K, Strasser F, Anker SD, Bosaeus I, Bruera E, Fainsinger RL, et al. Definition
540 and classification of cancer cachexia: an international consensus. Lancet Oncol. 2011;12:489-
541 95. doi:10.1016/S1470-2045(10)70218-7
542 8. Fearon KC, Glass DJ, Guttridge DC. Cancer cachexia: mediators, signaling, and
543 metabolic pathways. Cell Metab. 2012;16:153-66. doi:10.1016/j.cmet.2012.06.011
544 9. Tisdale MJ. Cachexia in cancer patients. Nat Rev Cancer. 2002;2:862-71.
545 doi:10.1038/nrc927

546 10. Aoyagi T, Terracina KP, Raza A, Matsubara H, Takabe K. Cancer cachexia, mechanism
547 and treatment. World J Gastrointest Oncol. 2015;7:17-29. doi:10.4251/wjgo.v7.i4.17
548 11. Fearon K, Arends J, Baracos V. Understanding the mechanisms and treatment options
549 in cancer cachexia. Nat Rev Clin Oncol. 2013;10:90-9. doi:10.1038/nrclinonc.2012.209
550 12. Mueller TC, Burmeister MA, Bachmann J, Martignoni ME. Cachexia and pancreatic
551 cancer: are there treatment options? World J Gastroenterol. 2014;20:9361-73.
552 doi:10.3748/wjg.v20.i28.9361
553 13. Kays JK, Shahda S, Stanley M, Bell TM, O'Neill BH, Kohli MD, et al. Three cachexia
554 phenotypes and the impact of fat-only loss on survival in FOLFIRINOX therapy for pancreatic
555 cancer. Journal of cachexia, sarcopenia and muscle. 2018;9:673-84.
556 14. Mantovani G, Maccio A, Lai P, Massa E, Ghiani M, Santona MC. Cytokine activity in
557 cancer-related anorexia/cachexia: role of megestrol acetate and medroxyprogesterone
558 acetate. Semin Oncol. 1998;25:45-52.
559 15. Straub RH, Cutolo M, Buttgereit F, Pongratz G. Energy regulation and neuroendocrine-
560 immune control in chronic inflammatory diseases. J Intern Med. 2010;267:543-60.
561 doi:10.1111/j.1365-2796.2010.02218.x
562 16. Argiles JM, Busquets S, Toledo M, Lopez-Soriano FJ. The role of cytokines in cancer
563 cachexia. Curr Opin Support Palliat Care. 2009;3:263-8. doi:10.1097/SPC.0b013e3283311d09
564 17. MacDonald N, Easson AM, Mazurak VC, Dunn GP, Baracos VE. Understanding and
565 managing cancer cachexia. J Am Coll Surg. 2003;197:143-61. doi:10.1016/S1072-
566 7515(03)00382-X

567 18. Carson JL, Hernandez M, Jaspers I, Mills K, Brighton L, Zhou H, et al. Interleukin-13
568 stimulates production of nitric oxide in cultured human nasal epithelium. In Vitro Cell Dev Biol
569 Anim. 2018;54:200-4. doi:10.1007/s11626-018-0233-y
570 19. Haslett PA. Anticytokine approaches to the treatment of anorexia and cachexia. Semin
571 Oncol. 1998;25:53-7.
572 20. Moldawer LL, Copeland EM, 3rd. Proinflammatory cytokines, nutritional support, and
573 the cachexia syndrome: interactions and therapeutic options. Cancer. 1997;79:1828-39.
574 21. Das SK, Eder S, Schauer S, Diwoky C, Temmel H, Guertl B, et al. Adipose triglyceride
575 lipase contributes to cancer-associated cachexia. Science. 2011;333:233-8.
576 22. Petruzzelli M, Schweiger M, Schreiber R, Campos-Olivas R, Tsoli M, Allen J, et al. A
577 switch from white to brown fat increases energy expenditure in cancer-associated cachexia.
578 Cell metabolism. 2014;20:433-47.
579 23. Taylor J, Uhl L, Moll I, Hasan SS, Wiedmann L, Morgenstern J, et al. Endothelial Notch1
580 signaling in white adipose tissue promotes cancer cachexia. Nature Cancer. 2023;4:1544-60.
581 24. Langer HT, Ramsamooj S, Dantas E, Murthy A, Ahmed M, Ahmed T, et al. Restoring
582 adiponectin via rosiglitazone ameliorates tissue wasting in mice with lung cancer. Acta
583 Physiologica. 2024;e14167.
584 25. Jang HJ, Kim HY, Lyu JH, Muthamil S, Shin UC, Kim HS, et al. Bee (Apis mellifera L.
585 1758) wax restores adipogenesis and lipid accumulation of 3T3-L1 cells in cancer-associated
586 cachexia condition. Food Science & Nutrition. 2024;
587 26. Tien S-C, Chang C-C, Huang C-H, Peng H-Y, Chang Y-T, Chang M-C, et al. Exosomal
588 miRNA 16-5p/29a-3p from pancreatic cancer induce adipose atrophy by inhibiting
589 adipogenesis and promoting lipolysis. Iscience. 2024;27:

590 27. Cook KB, Kazan H, Zuberi K, Morris Q, Hughes TR. RBPDB: a database of RNA-
591 binding specificities. Nucleic Acids Res. 2011;39:D301-8. doi:10.1093/nar/gkq1069
592 28. Gerstberger S, Hafner M, Tuschl T. A census of human RNA-binding proteins. Nat Rev
593 Genet. 2014;15:829-45. doi:10.1038/nrg3813
594 29. Pihlajamaki J, Lerin C, Itkonen P, Boes T, Floss T, Schroeder J, et al. Expression of the
595 splicing factor gene SFRS10 is reduced in human obesity and contributes to enhanced
596 lipogenesis. Cell Metab. 2011;14:208-18. doi:10.1016/j.cmet.2011.06.007
597 30. Brosch M, von Schonfels W, Ahrens M, Nothnagel M, Krawczak M, Laudes M, et al.
598 SFRS10--a splicing factor gene reduced in human obesity? Cell Metab. 2012;15:265-6; author
599 reply 7-9. doi:10.1016/j.cmet.2012.02.002
600 31. Huot ME, Vogel G, Zabarauskas A, Ngo CT, Coulombe-Huntington J, Majewski J, et al.
601 The Sam68 STAR RNA-binding protein regulates mTOR alternative splicing during
602 adipogenesis. Mol Cell. 2012;46:187-99. doi:10.1016/j.molcel.2012.02.007
603 32. Chou CF, Lin YY, Wang HK, Zhu X, Giovarelli M, Briata P, et al. KSRP ablation
604 enhances brown fat gene program in white adipose tissue through reduced miR-150
605 expression. Diabetes. 2014;63:2949-61. doi:10.2337/db13-1901
606 33. Dai N, Zhao L, Wrighting D, Kramer D, Majithia A, Wang Y, et al. IGF2BP2/IMP2-
607 Deficient mice resist obesity through enhanced translation of Ucp1 mRNA and Other mRNAs
608 encoding mitochondrial proteins. Cell Metab. 2015;21:609-21. doi:10.1016/j.cmet.2015.03.006
609 34. Siang DTC, Lim YC, Kyaw AMM, Win KN, Chia SY, Degirmenci U, et al. The RNA-
610 binding protein HuR is a negative regulator in adipogenesis. Nat Commun. 2020;11:213.
611 doi:10.1038/s41467-019-14001-8

612 35. Finan JM, Sutton TL, Dixon DA, Brody JR. Targeting the RNA-binding protein HuR in
613 cancer. Cancer Research. 2023;83:3507-16.
614 36. Michaelis KA, Zhu X, Burfeind KG, Krasnow SM, Levasseur PR, Morgan TK, et al.
615 Establishment and characterization of a novel murine model of pancreatic cancer cachexia. J
616 Cachexia Sarcopenia Muscle. 2017;8:824-38. doi:10.1002/jcsm.12225
617 37. Schweiger M, Eichmann TO, Taschler U, Zimmermann R, Zechner R, Lass A.
618 Measurement of lipolysis. Methods Enzymol. 2014;538:171-93. doi:10.1016/B978-0-12-
619 800280-3.00010-4
620 38. Rupert JE, Narasimhan A, Jengelley DH, Jiang Y, Liu J, Au E, et al. Tumor-derived IL-6
621 and trans-signaling among tumor, fat, and muscle mediate pancreatic cancer cachexia.
622 Journal of Experimental Medicine. 2021;218:e20190450.
623 39. Schweiger M, Eichmann TO, Taschler U, Zimmermann R, Zechner R, Lass A.
624 Measurement of lipolysis. In: Elsevier; 2014. pp. 171-93.
625 40. Liberzon A, Birger C, Thorvaldsdóttir H, Ghandi M, Mesirov JP, Tamayo P. The
626 molecular signatures database hallmark gene set collection. Cell systems. 2015;1:417-25.
627 41. Arneson-Wissink PC, Mendez H, Pelz K, Dickie J, Bartlett AQ, Worley BL, et al. Hepatic
628 signal transducer and activator of transcription-3 signalling drives early-stage pancreatic
629 cancer cachexia via suppressed ketogenesis. J Cachexia Sarcopenia Muscle. 2024;15:975-88.
630 doi:10.1002/jcsm.13466
631 42. Wu X, Gardashova G, Lan L, Han S, Zhong C, Marquez RT, et al. Targeting the
632 interaction between RNA-binding protein HuR and FOXQ1 suppresses breast cancer invasion
633 and metastasis. Commun Biol. 2020;3:193. doi:10.1038/s42003-020-0933-1

634 43. Fearon Kenneth CH, Glass David J, Guttridge Denis C. Cancer Cachexia: Mediators,
635 Signaling, and Metabolic Pathways. Cell Metabolism. 2012;16:153-66.
636 doi:10.1016/j.cmet.2012.06.011
637 44. Hwang JS, Lee WJ, Hur J, Lee HG, Kim E, Lee GH, et al. Rosiglitazone-dependent
638 dissociation of HuR from PPAR-γ regulates adiponectin expression at the posttranscriptional
639 level. The FASEB Journal. 2019;33:7707-20. doi:10.1096/fj.201802643r
640 45. Kang MJ, Ryu BK, Lee MG, Han J, Lee JH, Ha TK, et al. NF-κB Activates
641 Transcription of the RNA-Binding Factor HuR, via PI3K-AKT Signaling, to Promote Gastric
642 Tumorigenesis. Gastroenterology. 2008;135:2030-42.e3. doi:10.1053/j.gastro.2008.08.009
643 46. Grammatikakis I, Abdelmohsen K, Gorospe M. Posttranslational control of HuR
644 function. Wiley Interdisciplinary Reviews: RNA. 2017;8:e1372.
645 47. Huang Z, Liu S, Tang A, Wu X, Aube J, Xu L, et al. Targeting RNA-binding protein HuR
646 to inhibit the progression of renal tubular fibrosis. Journal of Translational Medicine.
647 2023;21:428.
648 48. Dong R, Chen P, Polireddy K, Wu X, Wang T, Ramesh R, et al. An RNA-Binding
649 Protein, Hu-antigen R, in Pancreatic Cancer Epithelial to Mesenchymal Transition, Metastasis,
650 and Cancer Stem Cells. Mol Cancer Ther. 2020;19:2267-77. doi:10.1158/1535-7163.Mct-19-
651 0822
652 49. von Haehling S, Coats AJ, Anker SD. Ethical guidelines for publishing in the Journal of
653 Cachexia, Sarcopenia and Muscle: update 2021. Wiley Online Library; 2021. pp. 2259-61.
654

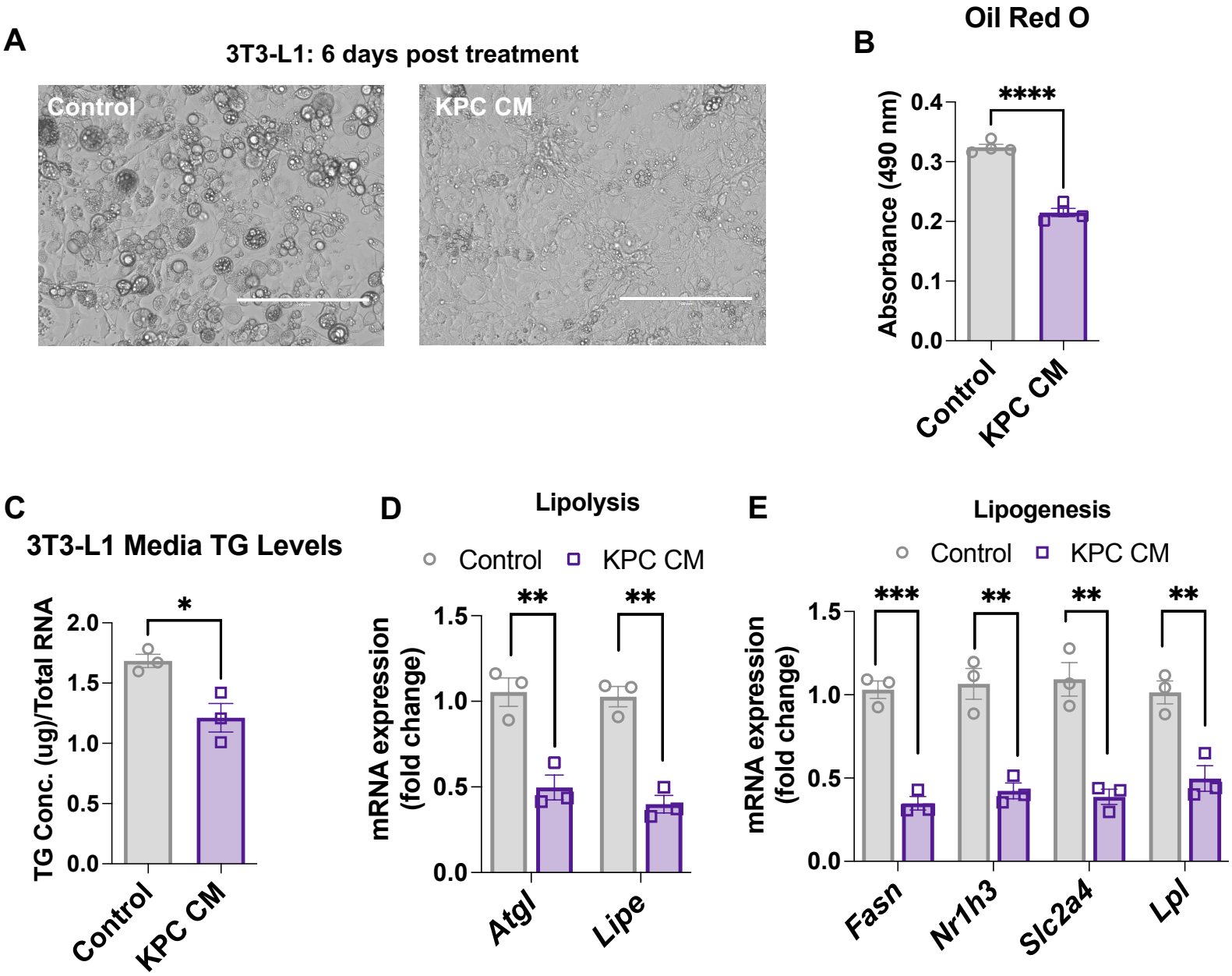
A
3T3-L1: 6 days post treatment
Control
KPC CM
B
Oil Red O
Absorbance (490 nm)
0.4
0.3
0.2
0.1
0.0
****
Control
KPC CM
C
3T3-L1 Media TG Levels
TG Conc. (ug)/Total RNA
2.0
1.5
1.0
0.5
0.0
*
Control
KPC CM
D
Lipolysis
Control
KPC CM
mRNA expression (fold change)
1.5
1.0
0.5
0.0
**
**
Atgl
Lipe
E
Lipogenesis
Control
KPC CM
mRNA expression (fold change)
1.5
1.0
0.5
0.0
***
**
**
**
Fasn
Nr1h3
Slc2a4
Lpl

Figure 1

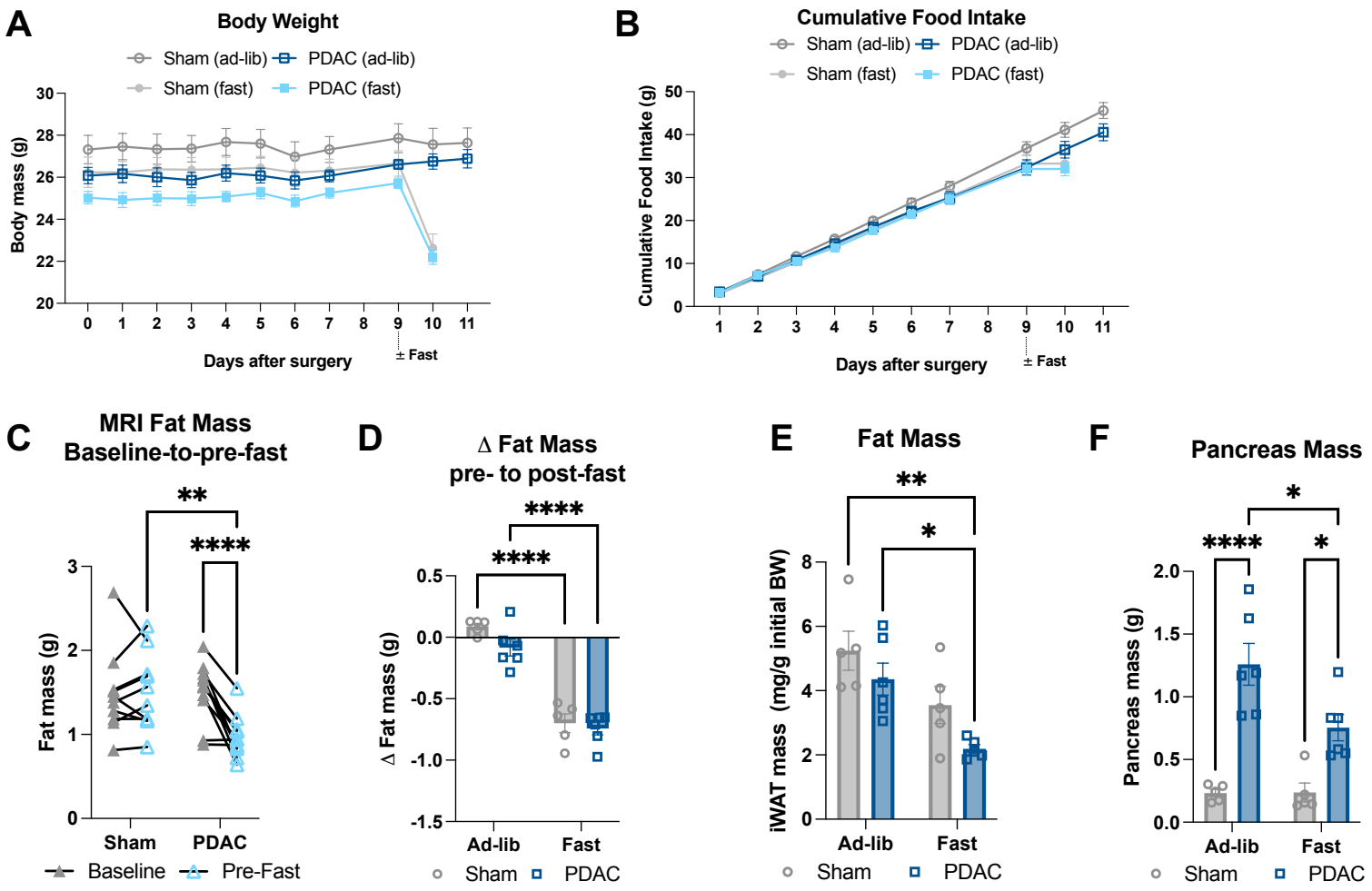
A
Body Weight
Sham (ad-lib)
PDAC (ad-lib)
Sham (fast)
PDAC (fast)
Body mass (g)
Days after surgery
± Fast
B
Cumulative Food Intake
Sham (ad-lib)
PDAC (ad-lib)
Sham (fast)
PDAC (fast)
Cumulative Food Intake (g)
Days after surgery
± Fast
C
MRI Fat Mass
Baseline-to-pre-fast
Fat mass (g)
Sham
PDAC
Baseline
Pre-Fast
D
Δ Fat Mass
pre- to post-fast
Δ Fat mass (g)
Ad-lib
Fast
Sham
PDAC
E
Fat Mass
iWAT mass (mg/g initial BW)
Ad-lib
Fast
Sham
PDAC
F
Pancreas Mass
Pancreas mass (g)
Ad-lib
Fast
Sham
PDAC

Figure 2

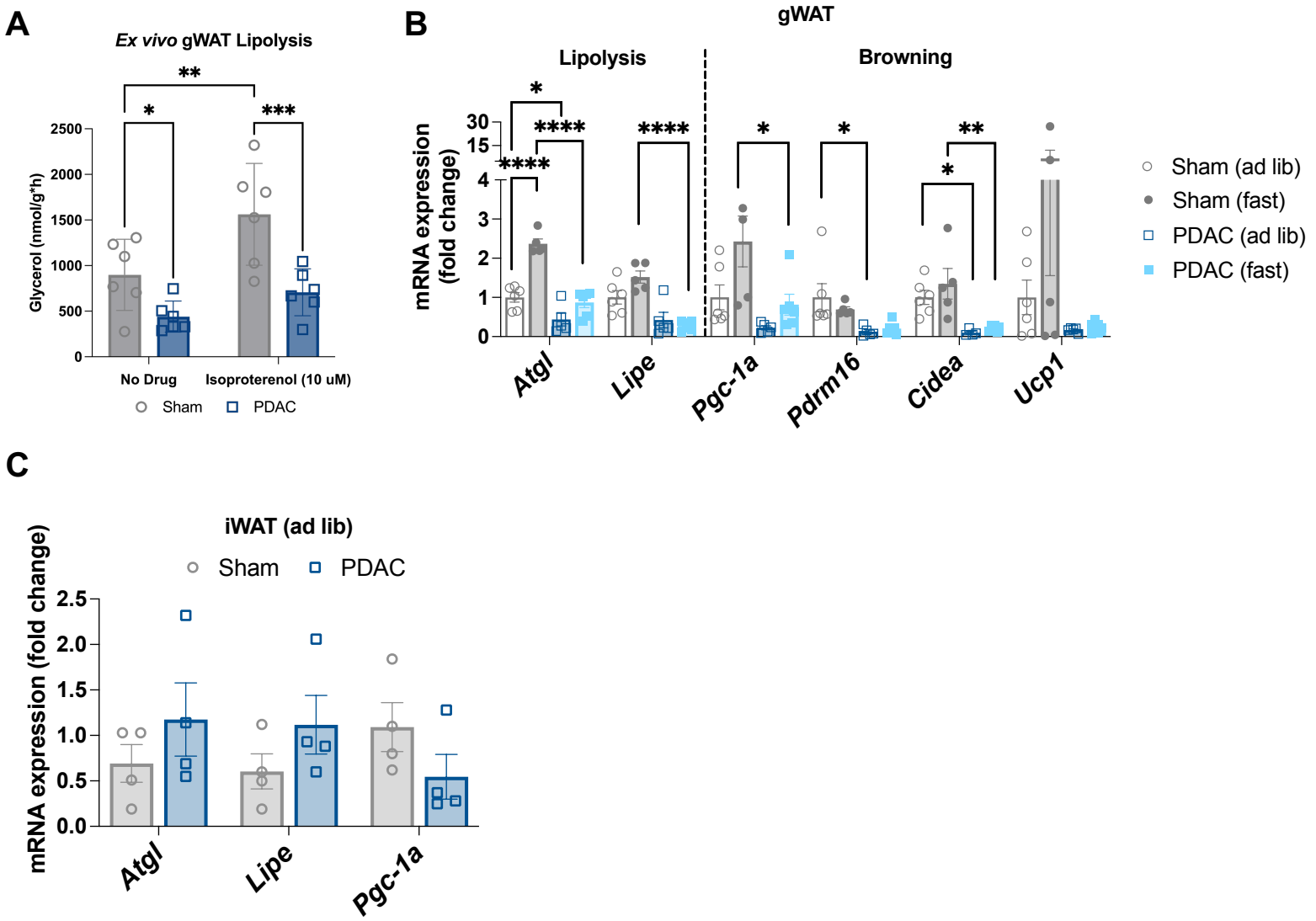
A
Ex vivo gWAT Lipolysis
Glycerol (nmol/g*h)
2500
2000
1500
1000
500
0
**
*
***
No Drug
Isoproterenol (10 uM)
Sham
PDAC
B
gWAT
Lipolysis
Browning
mRNA expression (fold change)
30
15
4
3
2
1
0
*
****
****
****
*
*
**
*
Atgl
Lipe
Pgc-1a
Pdrm16
Cidea
Ucp1
Sham (ad lib)
Sham (fast)
PDAC (ad lib)
PDAC (fast)
C
iWAT (ad lib)
Sham
PDAC
mRNA expression (fold change)
2.5
2.0
1.5
1.0
0.5
0.0
Atgl
Lipe
Pgc-1a

Figure 3

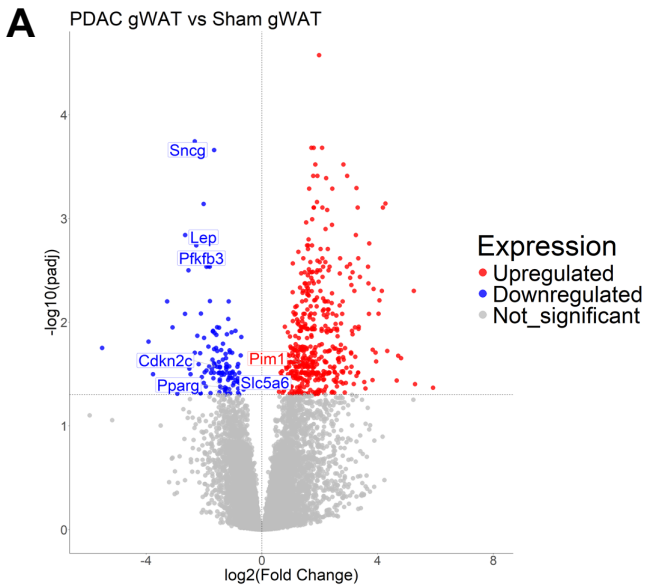
A
PDAC gWAT vs Sham gWAT
Sncg
Lep
Pfkfb3
Cdkn2c
Pparg
Pim1
Slc5a6
Expression
Upregulated
Downregulated
Not_significant
-log10(padj)
log2(Fold Change)

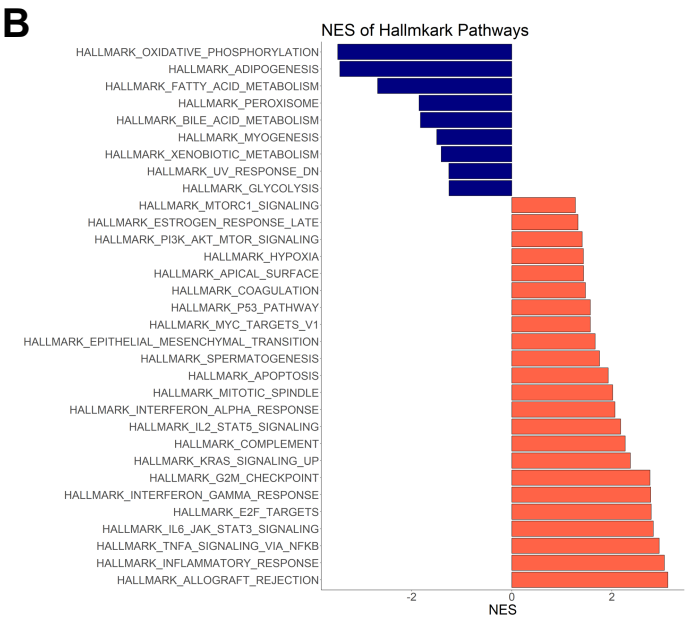
B
NES of Hallmkark Pathways
HALLMARK_OXIDATIVE_PHOSPHORYLATION
HALLMARK_ADIPOGENESIS
HALLMARK_FATTY_ACID_METABOLISM
HALLMARK_PEROXISOME
HALLMARK_BILE_ACID_METABOLISM
HALLMARK_MYOGENESIS
HALLMARK_XENOBIOTIC_METABOLISM
HALLMARK_UV_RESPONSE_DN
HALLMARK_GLYCOLYSIS
HALLMARK_MTORC1_SIGNALING
HALLMARK_ESTROGEN_RESPONSE_LATE
HALLMARK_PI3K_AKT_MTOR_SIGNALING
HALLMARK_HYPOXIA
HALLMARK_APICAL_SURFACE
HALLMARK_COAGULATION
HALLMARK_P53_PATHWAY
HALLMARK_MYC_TARGETS_V1
HALLMARK_EPITHELIAL_MESENCHYMAL_TRANSITION
HALLMARK_SPERMATOGENESIS
HALLMARK_APOPTOSIS
HALLMARK_MITOTIC_SPINDLE
HALLMARK_INTERFERON_ALPHA_RESPONSE
HALLMARK_IL2_STAT5_SIGNALING
HALLMARK_COMPLEMENT
HALLMARK_KRAS_SIGNALING_UP
HALLMARK_G2M_CHECKPOINT
HALLMARK_INTERFERON_GAMMA_RESPONSE
HALLMARK_E2F_TARGETS
HALLMARK_IL6_JAK_STAT3_SIGNALING
HALLMARK_TNFA_SIGNALING_VIA_NFKB
HALLMARK_INFLAMMATORY_RESPONSE
HALLMARK_ALLOGRAFT_REJECTION
NES

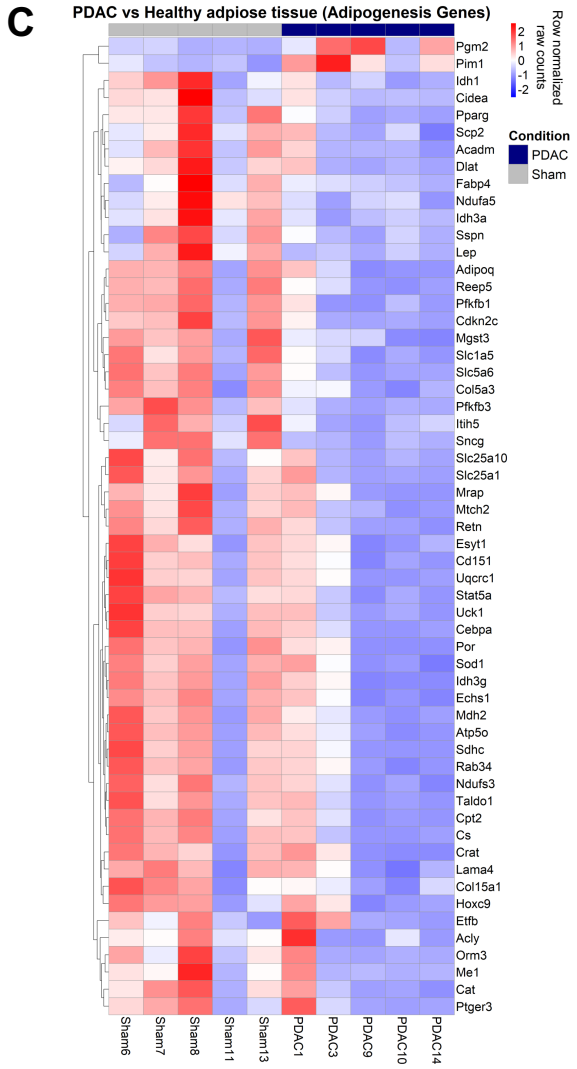
C
PDAC vs Healthy adpiose tissue (Adipogenesis Genes)
Row normalized raw counts
Condition
PDAC
Sham
Pgm2
Pim1
Idh1
Cidea
Pparg
Scp2
Acadm
Dlat
Fabp4
Ndufa5
Idh3a
Sspn
Lep
Adipoq
Reep5
Pfkfb1
Cdkn2c
Mgst3
Slc1a5
Slc5a6
Col5a3
Pfkfb3
Itih5
Sncg
Slc25a10
Slc25a1
Mrap
Mtch2
Retn
Esyt1
Cd151
Uqcrc1
Stat5a
Uck1
Cebpa
Por
Sod1
Idh3g
Echs1
Mdh2
Atp5o
Sdhc
Rab34
Ndufs3
Taldo1
Cpt2
Cs
Crat
Lama4
Col15a1
Hoxc9
Etfb
Acly
Orm3
Me1
Cat
Ptger3
Sham6
Sham7
Sham8
Sham11
Sham13
PDAC1
PDAC3
PDAC9
PDAC10
PDAC14

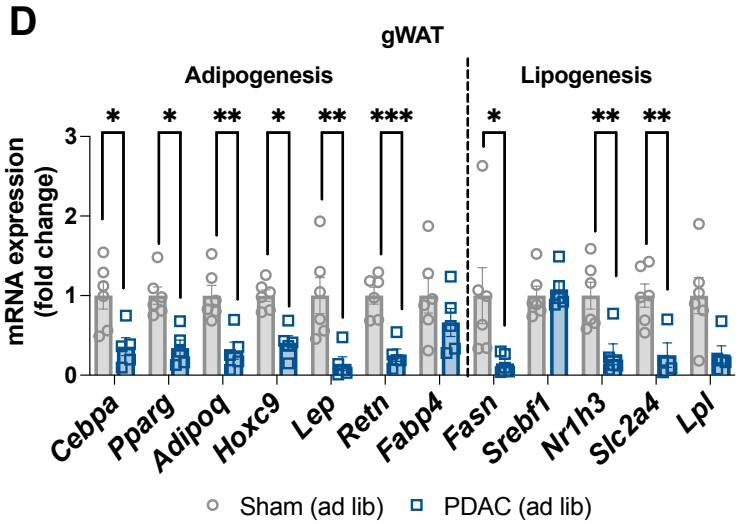
D
gWAT
Adipogenesis
Lipogenesis
mRNA expression (fold change)
Cebpa
Pparg
Adipoq
Hoxc9
Lep
Retn
Fabp4
Fasn
Srebf1
Nr1h3
Slc2a4
Lpl
Sham (ad lib)
PDAC (ad lib)

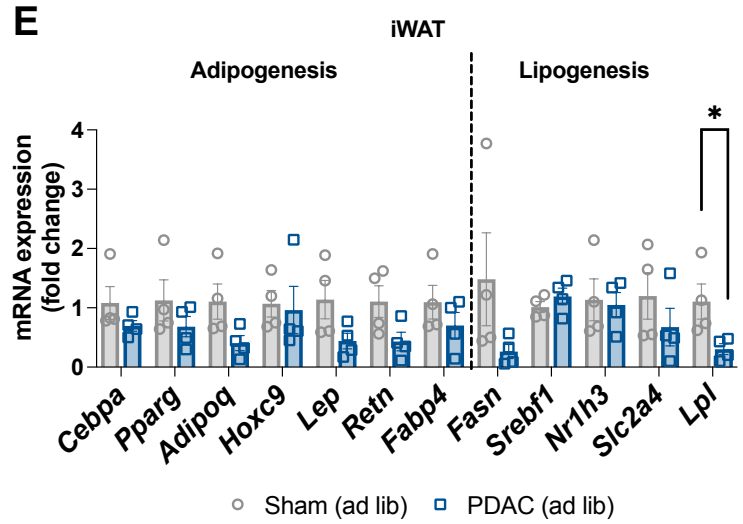
E
iWAT
Adipogenesis
Lipogenesis
mRNA expression (fold change)
Cebpa
Pparg
Adipoq
Hoxc9
Lep
Retn
Fabp4
Fasn
Srebf1
Nr1h3
Slc2a4
Lpl
Sham (ad lib)
PDAC (ad lib)

Figure 4

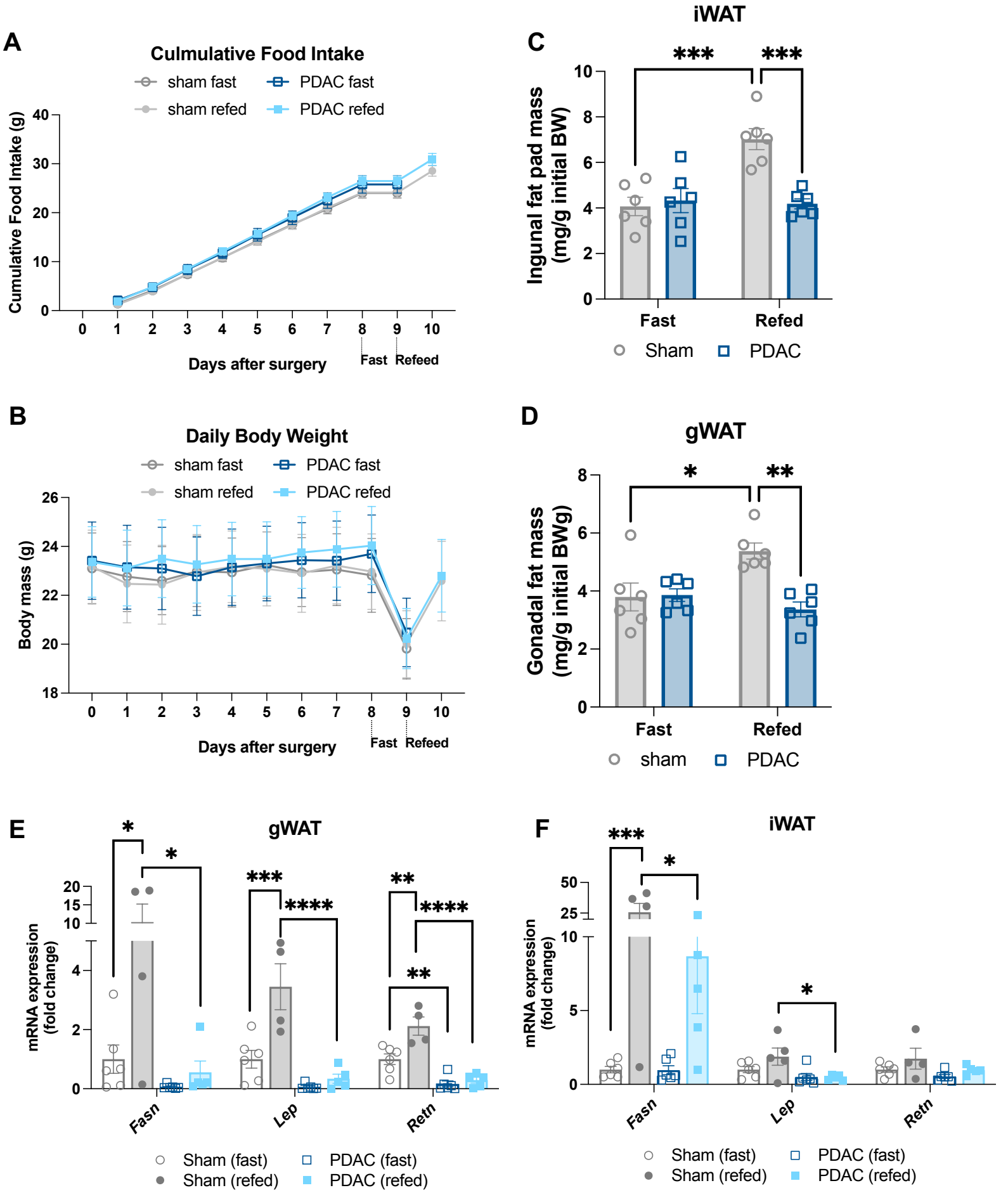
A
Culmulative Food Intake
sham fast
PDAC fast
sham refed
PDAC refed
Cumulative Food Intake (g)
Days after surgery
Fast
Refeed
B
Daily Body Weight
sham fast
PDAC fast
sham refed
PDAC refed
Body mass (g)
Days after surgery
Fast
Refeed
C
iWAT
Ingunal fat pad mass (mg/g initial BW)
Fast
Refed
Sham
PDAC
D
gWAT
Gonadal fat mass (mg/g initial BWg)
Fast
Refed
sham
PDAC
E
gWAT
mRNA expression (fold change)
Fasn
Lep
Retn
Sham (fast)
Sham (refed)
PDAC (fast)
PDAC (refed)
F
iWAT
mRNA expression (fold change)
Fasn
Lep
Retn
Sham (fast)
Sham (refed)
PDAC (fast)
PDAC (refed)

Figure 5

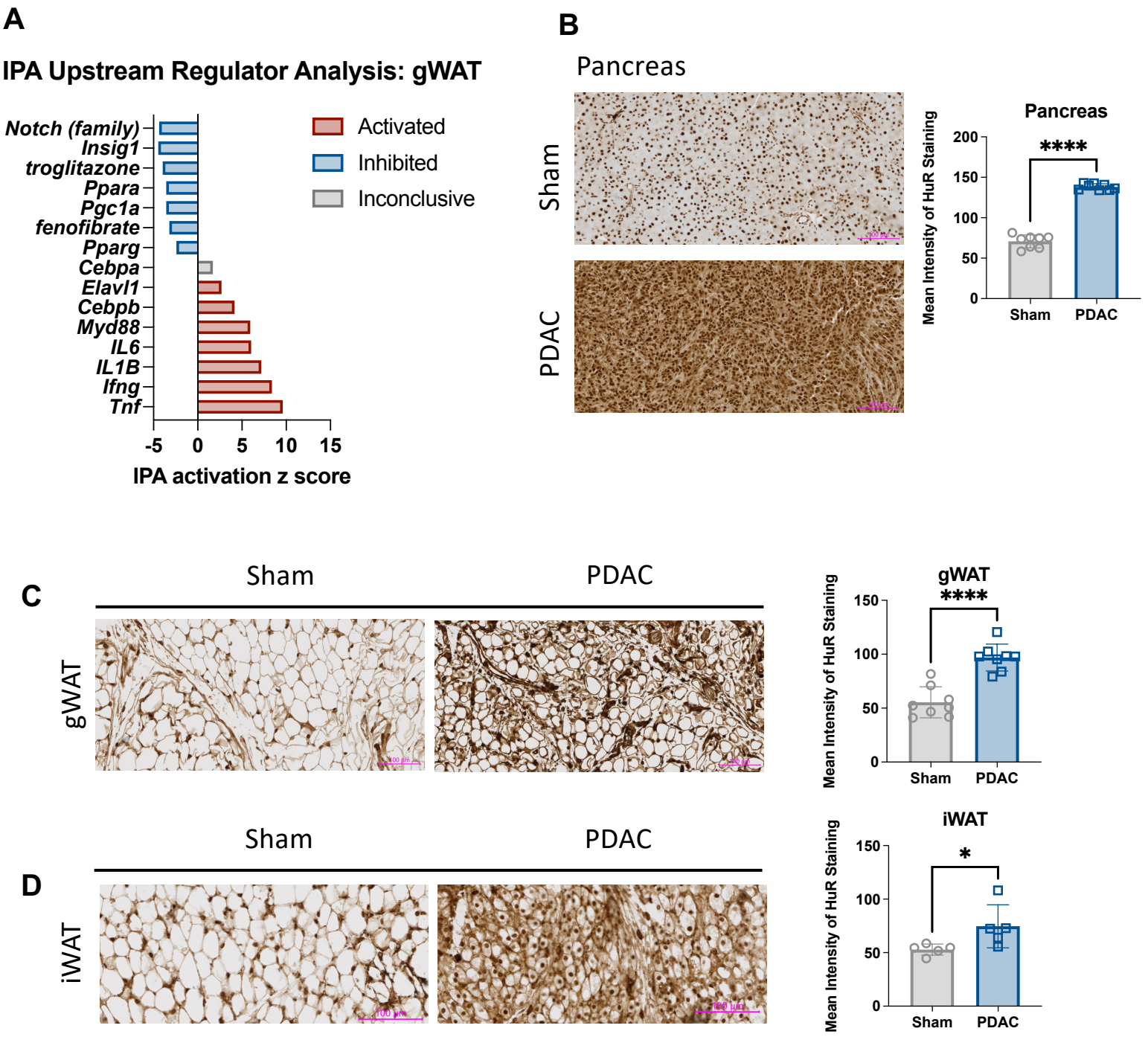
A
IPA Upstream Regulator Analysis: gWAT
Notch (family)
Insig1
troglitazone
Ppara
Pgc1a
fenofibrate
Pparg
Cebpa
Elavl1
Cebpb
Myd88
IL6
IL1B
Ifng
Tnf
Activated
Inhibited
Inconclusive
-5
0
5
10
15
IPA activation z score
B
Pancreas
Sham
PDAC
Pancreas
Mean Intensity of HuR Staining
200
150
100
50
0
****
Sham
PDAC
C
Sham
PDAC
gWAT
gWAT
Mean Intensity of HuR Staining
150
100
50
0
****
Sham
PDAC
D
Sham
PDAC
iWAT
iWAT
Mean Intensity of HuR Staining
150
100
50
0
*
Sham
PDAC

Figure 6

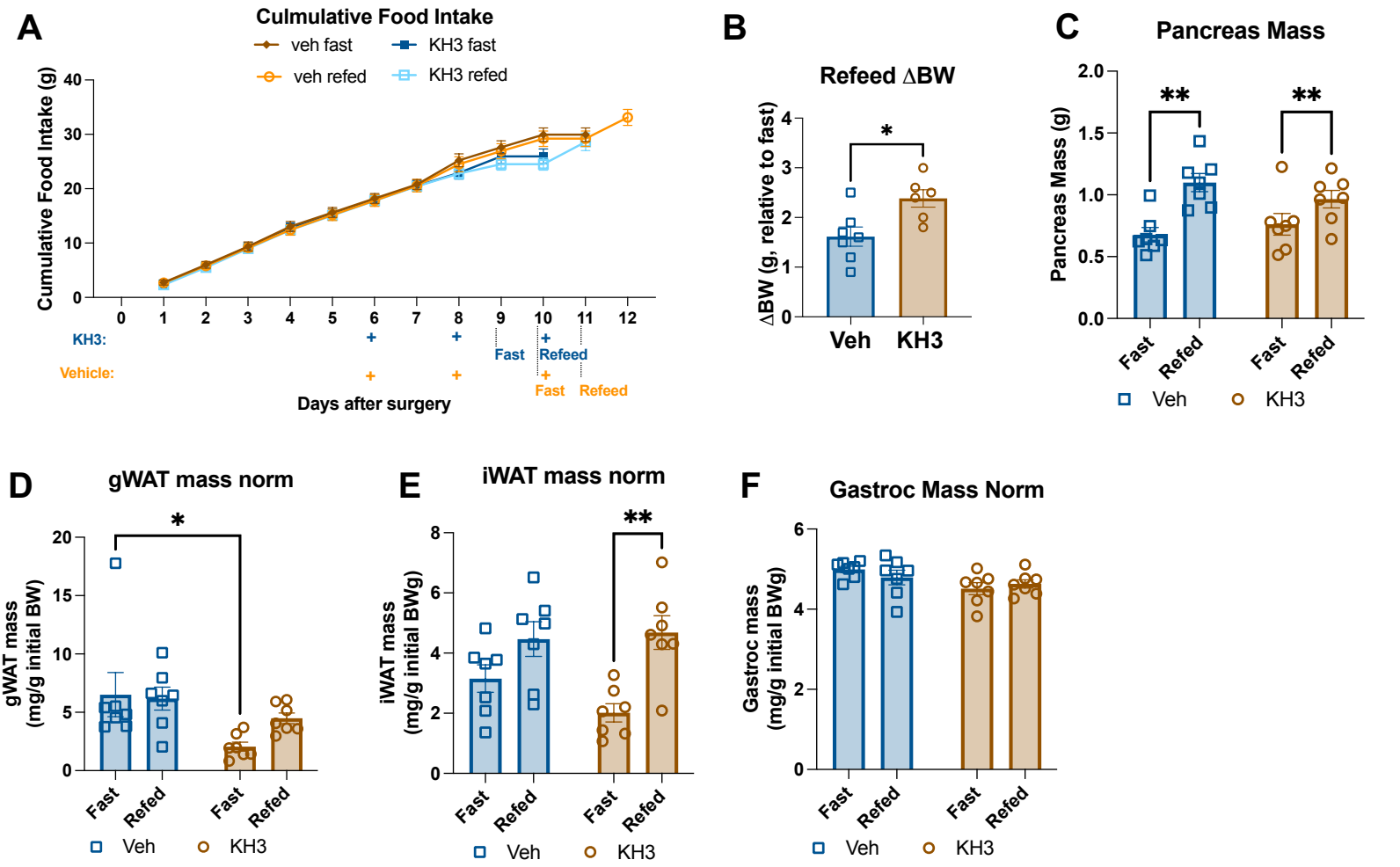
A
Culmulative Food Intake
veh fast
KH3 fast
veh refed
KH3 refed
Cumulative Food Intake (g)
KH3:
Vehicle:
Fast
Refeed
Days after surgery
B
Refeed ΔBW
ΔBW (g, relative to fast)
Veh
KH3
C
Pancreas Mass
Pancreas Mass (g)
Fast
Refed
Veh
KH3
D
gWAT mass norm
gWAT mass (mg/g initial BW)
E
iWAT mass norm
iWAT mass (mg/g initial BWg)
F
Gastroc Mass Norm
Gastroc mass (mg/g initial BWg)

Figure 7

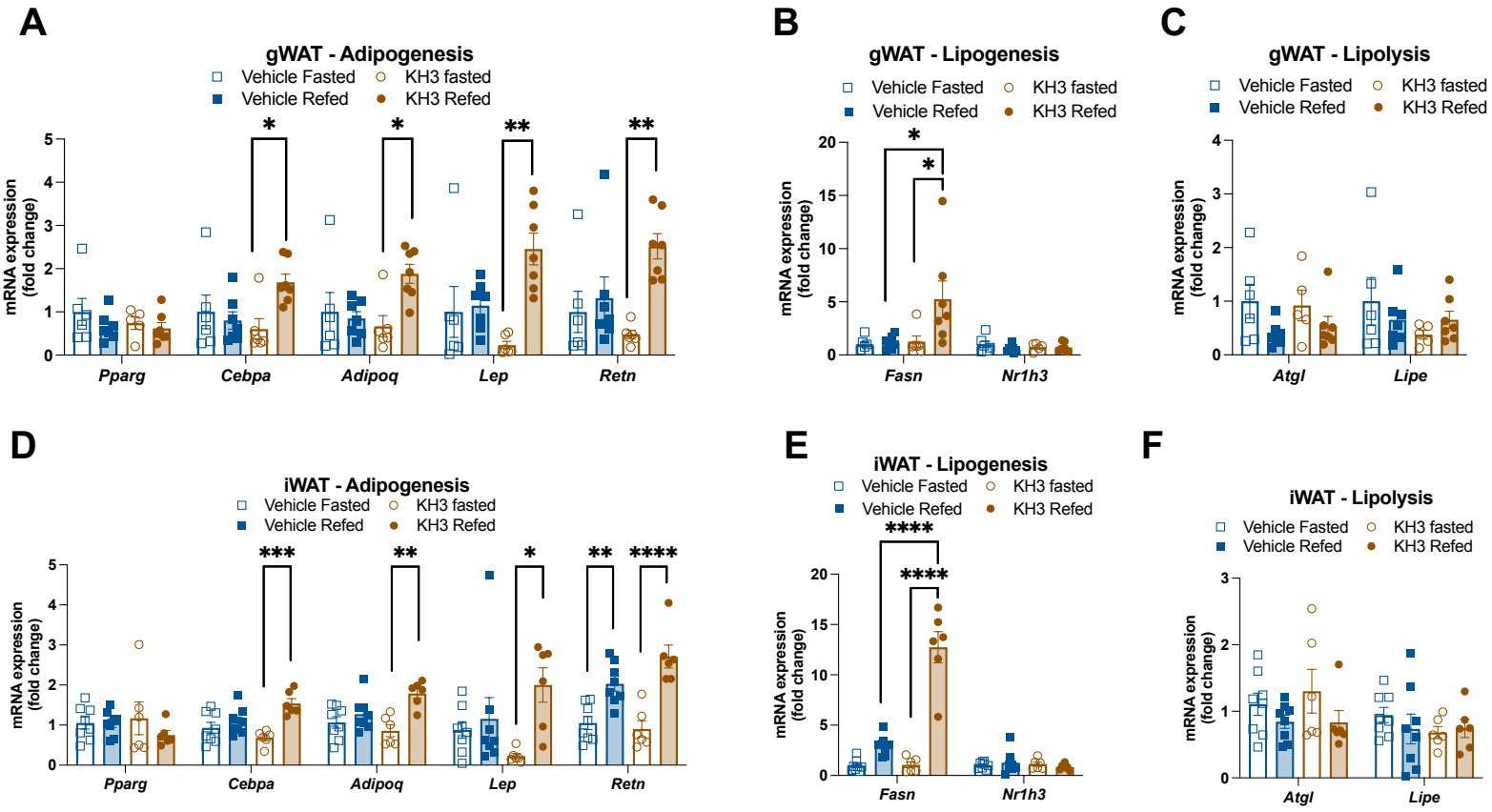
A
gWAT - Adipogenesis
Vehicle Fasted
Vehicle Refed
KH3 fasted
KH3 Refed
mRNA expression (fold change)
Pparg
Cebpa
Adipoq
Lep
Retn
B
gWAT - Lipogenesis
Fasn
Nr1h3
C
gWAT - Lipolysis
Atgl
Lipe
D
iWAT - Adipogenesis
E
iWAT - Lipogenesis
F
iWAT - Lipolysis

Figure 8